Involvement of Caveolin-1 in neurovascular unit remodeling after stroke: effects on neovascularization and astrogliosis

Running headline: Cav-1 in the neurovascular unit after stroke

Camille Blochet[1,2], Lara Buscemi[1], Tifenn Clément[2], Sabrina Gehri[1], Jérôme Badaut[2,3#] and Lorenz Hirt[1#]

1. Department of Clinical Neurosciences, CHUV, Lausanne, Switzerland

2. Brain Molecular Imaging lab, CNRS UMR 5287, INCIA, University of Bordeaux, France

3. Basic Science Department, Loma Linda University School of Medicine, Loma Linda, CA, USA

# Equally contributed to the work.

Correspondence

Jerome Badaut, PhD, Bordeaux University,

UMR CNRS 5287, 146 rue Leo Saignat,

33076 Bordeaux Cedex, France.

Email: jerome.badaut@u-bordeaux.fr

Lorenz Hirt, MD, Department of Clinical Neurosciences, CHUV

9 rue du Bugnon, Lausanne, Switzerland

Email: lorenz.hirt@chuv.ch

# Abstract

Complex cellular and molecular events occur in the neurovascular unit after stroke, such as Blood-Brain Barrier (BBB) dysfunction and inflammation that contribute to neuronal death, neurological deterioration and mortality. Caveolin-1 (Cav-1) has distinct physiological functions such as caveolae formation associated with endocytosis and transcytosis as well as in signaling pathways. Cav-1 has been proposed to be involved in BBB dysfunction after brain injury however, its precise role is poorly understood. The goal of this study was to characterize the expression and effect of Cav-1 deletion on outcome in the first week after a transient Middle Cerebral Artery Occlusion stroke model (tMCAO). We found increased Cav-1 expression in new blood vessels in the lesion and in reactive astrocytes in the peri-lesion areas. In Cav-1 KO mice, the lesion volume was larger and the behavioral outcome worse than in WT mice. Cav-1 KO mice exhibited reduced neovascularization and astrogliosis without formation of a proper glial scar around the lesion compared to WT mice at 3 days post injury coinciding with aggravated outcomes. Altogether, these results point towards a potential protective role of endogenous Cav-1 in the first days after ischemia by promoting neovascularization, astrogliosis and formation of a scar around the lesion.

# Introduction

Stroke is the third cause of death worldwide and the first cause of acquired disability in adults[1]. Overall, ischemic strokes represent approximately 85% of strokes[2]. Intravenous administration of recombinant tissue plasminogen activator was approved for the treatment of ischemic stroke in the United States in 1996 and by the European Union in 2003. More recently, it has been demonstrated that patients with ischemic stroke caused by a proximal occlusion in the anterior circulation benefit from endovascular thrombectomy[3]. Despite these improvements, an important number of patients do not benefit sufficiently from these treatments and remain disabled. Therefore, research aimed at discovering alternative therapies needs to be continued and neuroprotective agents should be re-examined as additional therapies to recanalization. An emerging concept is that protection could be achieved by studying and influencing the molecular mechanisms triggered not only in neurons after stroke but also in other cell types that likely participate in neuronal survival or play a role in repair mechanisms[4]. As such, endothelial cells and astrocytes, as part of the neurovascular unit (NVU)[5] could play a major role in preserving or recovering brain functions after stroke. The term neurovascular unit (NVU) alludes to brain blood vessels and emphasises the close physical and functional connection between brain tissue and blood vessels. Brain vasculature is anatomically distinct consisting of pericytes and astrocyte endfeet in addition to endothelial cells. Further, microglia and nerve endings contact brain vessels that collectively form the NVU. The BBB restricts passage of molecules from the blood circulation to the brain tissue as well as coordinating the exchange of ions, molecules and cells between the blood and brain. The presence and maintenance of the barrier properties by the NVU are critical for brain homeostasis and neuronal functioning[6]. After a stroke, brain tissue follows a remodeling process with neo-vascularization in the lesion core and formation of a glial scar around the core of the lesion[7, 8]. Therefore, NVU function is also probably central for brain tissue remodeling and potentially for brain plasticity and recovery.

Caveolins are transmembrane proteins involved in the formation of caveolae (plasma membrane invaginations or vesicles of 50 to 100 nm in size that serve as membrane organizing centers),

macromolecular transport and permeability, as well as signal transduction. Currently, there are three members of the caveolin family, Cav-1, Cav-2 and Cav-3, with highly conserved sequences across species[9]. In the brain, Cav-1 was initially believed to be restricted to endothelial cells, however it was then found in astrocytic cultures[10, 11] and in juvenile rat astrocytes after Traumatic Brain Injury (TBI)[12]. Caveolin proteins are key modulators of a variety of neuronal intracellular signaling pathways[13]. In caveolae, Caveolin-1 is the major multifunctional scaffolding protein that provides a docking site to anchor various proteins, thereby regulating a variety of signaling molecules and modulating downstream signaling pathways[14]. Caveolae are present in most cell types but are particularly abundant in endothelial cells, smooth and striated muscle cells, adipocytes[14] and astrocytes and neurons. Recently, new evidence has appeared on the beneficial role of caveolins in kidney, hind limb and cardiac ischemia models, indicating a ubiquitous role of caveolins in ischemic cell death[7]. Caveolae formation regulates several signaling pathways by caveolin oligomerization or directly by caveolin proteins via their scaffolding-binding domain[15]. Cav-1 for example, is known to down-regulate the activation of endothelial nitric oxide synthases (eNOS) resulting in inhibition of nitric oxide (NO) production[16]. Another study showed that Cav-1 activates matrix metalloproteinases (MMPs), especially MMP9 and MMP2, which are involved in the BBB opening after injury[17, 18]. The absence of Cav-1 could therefore limit the consequences of the lesion on BBB properties by a decrease of NO synthesis, limiting MMP9 production post-injury and preventing BBB rupture. However, the exact role of Cav-1 in modulating BBB integrity after brain injury is controversial. Notably, the expression of Cav-1 in brain microvessels is downregulated at three different time points after reperfusion after ischemia[17]. On the contrary, other immunofluorescence studies revealed an increase in Cav-1 expression in ischemic rat brains or an increase in the number of endothelial caveolae in a mouse model of ischemia and reperfusion[19, 20]. Moreover, Cav-1 deficiency increased cerebral ischemic injury in a permanent distal MCAO model[19]. Therefore, Cav-1 is likely to play an important role in NVU function via its involvement in BBB permeability but this probably depend on the injury model. Furthermore, it is now well established that the same protein can have several roles depending on its location with

respect to the lesion core and the time after the injury[14, 21]. Here, we address the role of Cav-1 by histological and immunohistochemical analysis of the NVU in the lesion core and perilesional tissue (penumbra) focusing on the new role of astrocytes after stroke and behavioral evaluation post-stroke which has never been reported in Cav-1 KO and WT mice from 6 hours to 7 days post-injury in a transient middle cerebral occlusion model.

## Material and Methods

Animal experiments and care complied with the Federal regulations and guidelines of the Swiss Veterinary Office and were approved by the Animal Care and Use Committee and registered as license VD2017.5. Animal reporting was according to the ARRIVE guidelines.

### Animal groups

We purchased Cav-1 KO mice in a C57Bl/6J background from Jackson Laboratory (JAX stock #007083) and bred them on site. We purchased male C57Bl/6J wild type (WT) mice (6 weeks-old) from Charles River. All animals used in experiments were housed for at least one week in a temperature-controlled animal facility on a 12-hours light-dark cycle with *ad libitum* access to food and water. Home cages contained standard bedding and enrichment material.

In our experimental design, we performed two sets of experiments with a total of 25 WT and 28 Cav-1 KO mice (Table 1):

| | WT | | Cav-1 KO | |
|---|---|---|---|---|
| | **tMCAO** | **Sham** | **tMCAO** | **Sham** |
| **Total** | **17** | **8** | **21** | **7** |
| **Sample Collection: Total** | **8** | **3** | **9** | **2** |
|    - Completed | 8 | 3 | 7 | 2 |
|    - Terminal endpoint reached | 0 | 0 | 2 | 0 |
| **Behavioral and lesion size study: Total** | **9** | **5** | **12** | **5** |
|    - Completed | 7 | 5 | 3 | 5 |
|    - Terminal endpoint reached | 1 | 0 | 6 | 0 |
|    - Found dead | 1 | 0 | 3 | 0 |

1) Behavioral evaluation and lesion size measurements with n=9 for WT and n=12 Cav-1 KO for tMCAO procedures. Sham experiments were also conducted in parallel with n=5 WT and n=5

Cav-1 KO mice. Animals were randomly assigned to sham or tMCAO procedures. Results of the sham animals are available as supplementary information online.

2) Immunofluorescence experiments with n=14 WT and n=17 Cav-1 KO animals collecting two to three different samples at the three different time points (sham and tMCAO at 6 hours, 1 and 3 dpi).

We tested animals in several behavioral tests every day after tMCAO and evaluated lesion size at 7 dpi. For immunofluorescence, animals were perfused (see below) at 6 hours, 1 and 3 dpi. Our veterinary authority approved the following humane termination endpoints: loss of righting reflex from 24h post-injury, status epilepticus, body weight loss of more than 25%. In the experiments described here, we had to terminate nine mice (1 WT and 8 Cav-1 KO mice).

**Transient Middle Cerebral Artery Occlusion (tMCAO) model**

We used the tMCAO model with the intraluminal suture method via the common carotid artery as previously described[22]. Briefly, mice were anesthetized with isoflurane (3% induction, 1.5-2% maintenance) and body temperature was maintained throughout surgery at 37±0.5°C with a heating pad (DC Temperature Controller, FHC). We monitored Cerebral Blood Flow (CBF) by Doppler flowmetry (Perimed system) using a flexible probe fixed onto the skull (1 mm posterior and 6 mm lateral from bregma). Baseline CBF was obtained before the carotid exposure. We induced ischemia by introducing an 11-mm silicone-coated 8–0 filament (Doccol Corp, USA) from the left common carotid artery into the internal carotid artery, advancing until we felt a resistance. We left the filament in place for 35 min. Successful ischemia was obtained when CBF during the tMCAO was below 20% of the baseline measurement and reperfusion had to achieve 50% of the baseline measurement. We excluded two WT animals and one Cav-1 KO from the experiment for not achieving reperfusion. We performed sham surgery under anesthesia, which consisted of placing the Doppler probe onto the skull and opening the neck to dissect the carotid arteries without filament insertion. After surgery, animals were maintained overnight in an incubator at

28°C. We assessed the coat, eyes and nose, neurological deficit, epileptic seizures, body weight loss and dehydration of all animals daily post-injury.

## Behavioral Assessment

### Neuroscore

We assessed the Neuroscore each day after injury; a modified version of the Bederson scale[23], according to the following ratings: no observable deficit: 0; failure to extend the right forepaw: 1; circling: 2; humane endpoint reached or death: 3. Intermittent circling was graded as 1.5[24].

### Rotarod test

We modified all behavioral tests assessing post-stroke deficits from Balkaya et al.[25].

For the rotarod test, briefly, mice were placed on an accelerating rotating cylinder (UgoBasile), and the longest latency to fall over three trials of maximum 900 seconds was recorded[24]. We trained mice three days before injury and tested on days 1, 3, 5 and 7 post-injury. We express performance as the percentage of the best performance from the training. Mice excluded before the end of the experiment due to sacrifice for humane reasons (see previously) were allocated a minimum score of 0 seconds in the following test-days to limit survival bias in the graphical representation and statistics.

### Adhesive Removal test

The animal was placed in a transparent Perspex box for 60 seconds for habituation. For the test, we applied a small piece of adhesive tape (rectangular piece 3 x 4 mm cut from Time®Tape, TimeMed Inc) under the forepaws while restraining the mouse. The order of placement (right or left forepaw first) was alternated for each trial. Directly after placing both adhesives, the experimenter pressed both forelimbs simultaneously to minimize bias. We then placed the mouse back into the Perspex box for 120 seconds and the time to contact and remove each adhesive tape was recorded and blindly scored using the Observer software (Noldus). Contact occurred when the paw was shaken or the mouth was used to touch the adhesive. We performed three consecutive trials for each mouse, every day of training or testing. Mice were trained three days

before injury and tested on days 2, 4 and 6 dpi. SG and CB scored blindly the time to contact and remove the adhesive on ipsilateral and contralateral paws and pooled data. We gave the maximum score of 120 seconds to mice excluded before the end of the experiment because of death or sacrifice for humane reasons to limit survival bias in the representation and the statistics.

## Lesion volume measurement

We froze brains in liquid nitrogen vapor after sacrifice. We collected 20 μm thick coronal sections using a cryostat (Leica CM3050) on Superfrost Plus® slides. Sections were stained with cresyl violet, then scanned with a stereomicroscope (Nikon SMZ 25) at 5x magnification and finally analyzed with ImageJ/FIJI software. CB quantitated infarction volumes, blinded to the animal group, on 12 coronal sections 720 μm apart. Infarction volumes were calculated by multiplying the sum of the infarcted areas on each section by the spacing distance.

## Immunofluorescence staining and image analysis

For tissue collection, mice were transcardially perfused first with PBS and then with 4% PFA at 4°C at a speed of 10 mL/min. Following overnight post-fixation in PFA, we cryoprotected brains in PBS with 30% sucrose for 48h, then froze them in isopentane cooled on dry ice. We collected 25 μm thick coronal sections using a cryostat and into cryoprotectant solution. Immunofluorescence staining was performed on free-floating sections with antigen retrieval with cold 33% acetic acid + 66% ethanol, blocked with 1% bovine serum albumin (BSA, Sigma Aldrich) + 5% horse serum + 0.1% Triton X100 solution for 1 hour at room temperature. Primary antibodies used were: Rabbit anti-Cav-1 (1:500, Abcam, cat # ab2910), Rat anti-CD31 (1:100, BD Biosciences, cat # 550274), Rabbit anti-GFAP (1:2000, Millipore Merck, cat # AB5804), Mouse anti-GFAP (1:2000, Millipore Merck, cat # MAB3402), Mouse anti-GS (1:1000, Millipore Merck, cat # MAB302), Mouse anti-MAP2 (1:500, Millipore Merck, cat # MAB3418), Rabbit anti-Ki67 (1:200,Thermofisher, cat # RM-9106-R7). Primary antibodies were incubated in antibody solution (1% BSA + 0.3% Triton X100 in PBS) overnight at 4ºC. Appropriate secondary antibodies, all

Alexa Fluor® labeled (Invitrogen) were incubated in antibody solution together with DAPI as nuclear counterstain for one hour at room temperature. Sections were mounted on SuperFrost Plus® slides (Fischer Scientific) with FluorSave medium (Calbiochem) and coverslipped.

We captured images of whole-coronal brain sections using a slide-scanner (Zeiss AxioScan Z1) at 10x magnification. We acquired stained caveolin proteins and other cellular markers in the ipsilateral and contralateral striatum to the lesion with a confocal microscope (Zeiss LSM 710 Quasar) at 67x magnification.

Images for the vessel density analysis and the quantification of Ki67 were acquired with the same confocal microscope at 40x magnification. Vessel density analysis was performed using the vessel density plugin available for Fiji. The quantification of Ki67 positive nuclei was done on averaged z-projections using Fiji on stacks of 15 to 17 images with 1µm spacing on 3 images per animal with 3 animals in each group (WT and Cav-1 KO).

Stacks of images for the morphological analysis were acquired with an epifluorescence microscope (Zeiss Imager Axio Z1) at 40x magnification. The morphological analysis of astrocytes was performed by TC using Fiji's bandpass and unsharp mask filtering, binarization, skeletonization and skeleton analysis as described in Morrison et al.[26] on the averaged z-projections on n=4 areas per animal with 3 animals per group. Quantification of the Ki67 positive nuclei and analysis of the morphology of astrocytes were performed blinded to the group of mice.

### Western Blots

Protein were prepared from frozen cryostat sections collected for WT Sham and tMCAO where ischemic was separated from contralateral non-ischemic hemisphere of the brain. Samples were homogenized in cold modified Bonny lysis buffer containing protease and phosphatase inhibitors. Protein quantification was performed with a Bradford Kit (Bio-Rad). Proteins were then separated on gels (NuPAGE 10% Bis-Tris Gel, cat # NP0302BOX) and transferred to PVDF membranes. The membranes were then placed in blocking solution (Li-Cor Odyssey Blocking buffer, Part No:927-4000) for 1 hour. The membranes were incubated with Cav-1 (1:1000, Abcam, cat # ab2910) and

α-tubulin (alpha-tubulin (TU-02), 1:2000, Santa Cruz Biotech, cat # sc-8035) primary antibody overnight at 4°C. Afterward, the membranes were washed in PBS + 0.05% Tween and finally incubated 1 hour at room temperature with IR-conjugated secondary antibodies (Odyssey IRDye® Goat anti-Mouse 800 CW and Goat anti-Rabbit 680LT, Li-Cor). The Li-cor system was used to detect bound primary antibody. Western blots for Cav-1 were quantitated with Fiji software using the mean gray value of each band and compared using one-way ANOVA.

## Statistical analysis

We performed all measurements and analyses without knowledge of the group and statistical analyses using Prism software (GraphPad). We represent data as box and whiskers plots, showing the median, minimal and maximal values as well as individual data points. Bar graphs are expressed as mean ± Standard Deviation (SD) and individual data points are displayed. We compared the survival of the two groups statistically with the Mantel-Cox test. We carried out two-group comparisons with the Student unpaired t-test after testing Gaussian distribution and similar standard deviation for both populations. We analyzed behavioral tests performed with the same groups of animals over several days with 2-way ANOVA for repeated measures with Holm-Sidak multiple comparison post-hoc test. Statistical significance was set at * p<0.05, ** p<0.01, *** p<0.001 or **** p<0.0001.

## Results

### *Expression of Caveolin-1 in endothelial cells and reactive astrocytes*

We investigated the expression and cellular localization of Cav-1 in ipsilateral and contralateral hemispheres to the lesion using Western Blot and double-immunostaining with anti-CD31 (endothelial cell marker), anti-Glutamine Synthetase (GS, pan-astrocyte marker) or anti-Glial Fibrillary Acidic Protein (GFAP, reactive astrocyte marker) and anti-Cav-1 in WT coronal brain sections 3 days after tMCAO (Figure 1). Quantification of Cav-1 protein in the Western Blot (Figure 1a) revealed an up-regulation of Cav-1 in the ipsilateral side compared to the contralateral side to the lesion using one-way ANOVA (F=11.45 , p=0.0090). We found a co-localization of Cav-1- and CD31 immunolabeling, in the striatum ipsilateral and contralateral to the lesion (Figure 1c, left panel compared to Figure 1d, right panel). Cav-1 also co-localized with GS positive astrocytes in the ipsilateral striatum and to a lesser extent on the contralateral side to the lesion (Figure 1e-f). Finally, in the peri-lesion area in the ipsilateral hemisphere (Figure 1g, left panel), we observed Cav-1 in some reactive astrocytes, stained by GFAP-immunoreactivity. In the contralateral hemisphere (Figure 1h, right panel), only a few astrocytes in the striatum were GFAP positive, but co-localization with Cav-1 was observed here too. Negative controls on Cav-1 KO samples and triple staining of Cav-1 with microglial marker Iba-1 and neuronal marker NeuN available online in supplementary (respectively Supplementary figures 1 and 2)

These results provide evidence of the modification of Cav-1 expression in the neurovascular unit after stroke. More specifically, we saw enhanced Cav-1 in endothelial cells in the lesion and interestingly, presence in reactive astrocytes in WT animals after stroke.

### *Outcome assessment*

### *Assessment of survival and lesion size*

We used Cav-1 KO mice in order to investigate the impact of the absence of Cav-1 on outcome after tMCAO.

In both experimental groups (WT and Cav-1 KO) not all animals reached the set sacrifice time point of 7 days post-injury (dpi). We sacrificed some animals, mainly from the Cav-1 group, earlier according to predetermined termination criteria or found them dead. Following 35 min tMCAO, most of the WT mice survived 7 days (7/9). However, Cav-1 KO mice showed a significantly decreased survival rate compared to WT (3/12) quantified using a Kaplan-Meier curve (Figure 2a, Mantel-Cox test ($\chi^2$=4.603, p=0.0319)). It is to note that the loss of Cav-1 did not pre-dispose mice to lethality without the tMCAO. All animals exposed to sham injuries (anesthesia and carotid dissection without insertion of the filament) survived for the planned duration of 7 days after injuries and performed as well as WT in the behavioral tasks (Supplementary Figure 3).

In agreement with the decreased survival rate, the lesion volume measured on cresyl violet stained sections at the time of sacrifice (3 to 7 dpi) was significantly larger in the Cav-1 group compared to WT (65.73 ± 27.33 mm$^3$ (mean ± SD) versus 33.33 ± 18.67 mm$^3$ respectively Figure 2b, unpaired t-test (t= 2.44, p=0.0326)). The increased volume also persisted when we took into account the edema by measuring the size of the ischemic lesion compared to the total size of the brain.

The evolution of the lesion pattern over time after reperfusion at 6h, 24h and 3 days was evaluated in WT and Cav1-KO mice using microtubule associated protein 2 (MAP-2) staining of neurons (Figure 2c). A decreased area of MAP-2-labeling revealed the lesion core highlighted by a yellow dotted line. The surface area of decreased MAP-2 staining appeared already larger in Cav-1 KO animal sections compared to WT as early as 6 hours post-injury. In the Cav-1 KO sections, we observed decreased MAP-2 labeling in the striatum as well as in a large part of the cortex at 6h after reperfusion while, in the WT group at 6 hours after tMCAO, the decrease in MAP-2 staining was limited to the striatum.

Overall, these results suggest that the presence of Cav-1 attenuated and/or delayed the development of the ischemic lesion.

*Assessment of sensorimotor deficits*

We determined general neurological status (righting reflex, forepaw extension and spontaneous locomotor activity) using the neuroscore, a modified version of the Bederson scale[23]. The neuroscore was assessed every single day after the stroke (see supplementary data, Supplementary Figure 4), however only the scores obtained at 1, 4 and 7 dpi are shown in Figure 3a for clarity. As outlined in the methods, behavioral performances were analyzed statistically with ANOVA, using either days or experimental groups as variables. Globally, there was a significantly higher proportion of animals exibiting neuroscore improvement over time after injury in WT mice compared to KO mice (two-way ANOVA with repeated measures, percentage of total variation: 8.061%, p<0.0001). The Cav1-KO mice showed the opposite trend, with a higher number of animals developing a more severe score than the WT group (Figure 3a). There was a signifcant difference between experimental groups: WT and Cav-1 KO (percentage of variation: 13.02%, p=0.0367) as well as on the interaction between experimental group and day variables (percentage of variation: 6.88%, p=0.0001).

The time spent on the rotarod before falling is presented as percentage of the best perfomance (or longest latency to fall) measured before stroke onset for each animal in Fig 3b. We recorded rotarod performance at 1, 3, 5 and 7 dpi (Figure 3b). At one dpi, both WT and Cav-1 animals performed below 50% of their best baseline. On day 3 dpi, WT animals improved to 73.14 ± 34% (mean ± SD) whereas Cav-1 KO animals only improved to 45.43 ± 45%. WT animals performed similarly at days 5 and 7 dpi while Cav-1 KO performance decreased due to the increased mortality. The difference between experimental groups (WT versus Cav-1 KO animals) was significant with the two-way ANOVA with repeated measures (percentage of total variation: 13.79%, p=0.0117).

We used the adhesive removal test to assess fine sensorimotor skills involving mouth and digits. We present the time to contact or remove the adhesive as the difference between the testing time and the best baseline time measured before stroke onset for each animal, with results from the paw ipsilateral to the lesion pooled with the results of the contralateral paw. The mean time to

contact (Figure 3c) and remove (Figure 3d) the adhesive was increased for both groups at 3 dpi. Moreover, Cav1-KO mice on average took longer to contact and remove the adhesive than WT mice at this time-point. The ANOVA with repeated measures for contact times was significant between days of testing post-stroke (percentage of variation: 16.24%, p<0.0001) and between WT and Cav-1 KO groups (percentage variation 6.031%, p=0.0293) but also the interaction between days and experimental groups was significantly different (percentage of variation: 4.117%, p=0.0166). Significant differences for the removal time were also seen for the effect of days (percentage of variation: 3.987%, p=0.0202) and experimental groups (percentage of variation: 15.48%, p=0.0018) but not for the interaction of the two variables.

In summary, Cav-1 KO mice exhibit worse functional outcome than WT mice in accordance with the larger lesion volumes observed. All together, these results suggest a protective role for Cav-1 protein after stroke.


## *Assessment of neovascularization*

In Figure 4a and b we show CD31-labeling (red) having brighter staining in the lesion core compared to the contralateral area at 3 dpi in both WT and Cav-1 KO mice, suggesting an increase of blood vessel CD31-reactivity (Figure 4a, b). This enhanced labeling could reflect neovascularization so we used Ki67, a marker of cell proliferation in combination with CD31 to test this. Coronal brain sections showed Ki67 staining in the ischemic lesion in both groups (Figure 4c, d). Interestingly, the number of Ki67 positive nuclei appeared higher in WT animals (Figure 4c) compared to Cav-1 KO animals (Figure 4d). We confirmed this on images at 40x magnification where we saw a significantly higher number of CD31 positive cells with Ki67 labeled nuclei (Figure 4e,g), in WT than in Cav-1 KO mice, suggesting reduced cell proliferation in Cav-1 KO after stroke. On the vessel density analysis (Figure 4f), more area of vasculature was found in the WT compared to the Cav-1 KO images (unpaired t-test: t=3.485, p=0.0019). On quantification (Figure 4g), the number of Ki67-positive nuclei per area was significantly higher in WT with 49.33 ± 12.1

Ki67-positive nuclei (mean ± SD) compared to Cav-1 KO animals, 21.56 ± 6.15 Ki-positive nuclei (unpaired t-test, t=6 and p<0.0001) in images at 20x magnification. Similarly, the number of Ki67-positive nuclei in endothelial cells was significantly higher with 21.1 ± 4.5 positive nuclei per area for the WT and 13.44 ±3.82 (Mean ±SD) for the Cav-1 KO (t-test, t=2.498, p=0.0238).

Our results show that the absence of Cav-1 affects the number of proliferating endothelial cells in the lesion and this may impair the process of neovascularization observed in the core of the lesion after stroke.

## Cav-1 and astrocyte reactivity

We observed the presence of Cav-1 in reactive astrocytes after stroke (Figure 1c), and went on to determine for the first time possible effects of Cav-1 absence on astrogliosis and formation of the glial scar. We performed double labelling with MAP-2 (green) to delineate the lesion area and GFAP (red) to stain reactive astrocytes in brain sections from WT and KO animals collected at 6h, 24h and 3 dpi, to establish a time-course of the astrocyte changes in relation to the ischemic lesion on coronal sections (Figure 5a). We observed reactive astrocytes with increased GFAP staining in the peri-lesion areas in WT samples, with an obvious increase at 3 dpi compared to 6 and 24h. Interestingly, the Cav-1 KO mice did not display such a noticeable increase in GFAP labeling in the ischemic peri-lesion at 3 dpi nor at earlier time points. Cell proliferation revealed by the Ki67 marker identified some new cells as GFAP positive cells indicating the proliferation of reactive astrocytes in the peri-lesion (Figure 5b). We analyzed possible morphological differences in GFAP-positive astrocytes and their processes between the two groups of mice on images at higher magnification (40x). GFAP images were taken from z-projections made from stacks of images that were filtered (Figure 5c) and skeletonized. In the Cav-1 KO mice, the GFAP immunolabelled reactive astrocytes showed a distinct morphology to the WT group, with shorter processes (arrowheads) and less branches. We confirmed this visual impression by morphology analysis (Figure 5d). The total number of GFAP positive cells was changed between the groups

with more astrocytes in the Cav-1 KO group compared to the WT (t=2.196, p=0.0372). The number of endpoints of the astrocytes showed a tendency to decrease in Cav-1 KO images compared to WT (t=1.893, p=0.0695). Similarly, the total length of astrocyte branches (272 ± 42.77 for WT versus 239 ± 30.5 for Cav-1 KO) and the maximum branch length (48.66 ± 6.25 for WT versus 41.21 ± 6.86 for Cav-1 KO) were significantly decreased in the Cav-1 KO animals (t=2.498, p=0.0192 and t=2.897, p=0.0076 respectively, n= 4 images per animal in n=3 animals per group).

All together, these results point towards a change in the pattern and the distribution of reactive astrocytes with morphological differences in the absence of Cav-1.

## Discussion

The NVU has been proposed as a key element for future development of new treatments for stroke and other brain disorders[5]. We and others previously showed changes of Cav-1 expression in the NVU in various brain disorders[12, 19, 27], however, the changes in Cav-1 expression and the role of the protein in stroke is not clear at present[7]. To address this question, we studied changes in Cav-1 expression in the NVU over time after tMCAO, then compared the functional outcome as well as changes at the cellular level in WT and genetically modified Cav-1 KO mice. Overall, in this study, the absence of Cav-1 is associated with (1) an increased mortality and a larger lesion volume after tMCAO, (2) a more severe functional outcome with sensorimotor deficits assessed by the neuroscore, rotarod and adhesive removal test behavioral tests, (3) increased - proliferation of endothelial cells, (4) changes in reactive astrocytes morphology and distribution in the peri-lesion. The results presented here provide several novel and important findings regarding the behavior and the role of astrocytes in Cav-1 KO mice after ischemic stroke. One of the important findings in the present study is the modification of reactive astrocyte morphology and distribution in the absence of Cav-1.

We believe that the presence of Cav-1 is important for limiting the progression of the pathology after stroke onset by facilitating (1) neovascularization in the ischemic lesion and (2) astrogliosis and scar formation in the perilesional tissue which has never been considered after stroke so far (Figure 6). Our work suggests a decisive role of Cav-1 in these two processes contributing to tissue repair.

### Presence of Cav-1 benefits recovery post-stroke:

Various studies have shown changes in Cav-1 expression in several preclinical models of brain disorders with a dual interpretation of its role[7, 18]. This is true for stroke research where preclinical studies used a variety of animal models with conflicting results reporting deleterious or beneficial roles of Cav-1 after stroke. Here we chose the filament tMCAO model as the middle cerebral artery is the most commonly affected blood vessel in human ischemic stroke[28] and this

model has been used in many studies addressing pathophysiological processes or neuroprotective agents[22]. This model is also more physiological than the previously used model[19] of permanent distal MCAO which requires a craniotomy and can therefore impact early post-stroke behavioral assessment. Different lengths of occlusion have been tested in our lab and the 35 minutes occlusion was determined as a good compromise between variability of lesion sizes and severity in the C57Bl6/J WT mice. In this model, Cav-1 KOs displayed larger lesion sizes at time of sacrifice compared to WTs, suggesting a beneficial role of Cav-1 in tMCAO. We observed a difference between groups as early as 6 hours after injury, with a more prominent loss of neurons in the absence of Cav-1.

The major preclinical outcome measures for stroke pharmacotherapy studies are final lesion size and sensorimotor neurological deficits. The latter are more clinically relevant and also more challenging to accurately assess as deficits can rapidly resolve in rodent models[9]. A broad variety of tests have been described to assess post-stroke deficits[25]. To our knowledge, we are the first to assess and describe sensorimotor deficits in Cav-1 KO mice following stroke. We chose three tests (Neuroscore, rotarod and adhesive removal) in order to discriminate between general neurological deficits (neuroscore), locomotor activity (rotarod) and fine movements (adhesive removal). In the Cav-1 KO group, at all time points, the neuroscore was worse, the time to fall from the rotarod shorter and the time to contact and remove the adhesive longer than in the WT group. Overall, these three outcome assessments highlighted greater sensorimotor deficits for the Cav-1 KO group in agreement with the large lesion volumes. Others have reported neurological abnormalities including clasping, abnormal spinning, muscle weakness, reduced activity and gait abnormalities in Cav-1 KO mice[29, 30]. However, we did not observe this and found no significant differences in the three behavioral tests used in this study between WT and Cav-1 KO mice after sham injuries (Supplementary Figure 4).

Our results are in agreement with a previous study[19] where Cav-1 KO mice had increased lesion volumes at a short time point in a model of permanent distal MCAO (MCA sutured locally after a craniotomy). In the cited work, the authors suggested an important role of increased Cav-1 at 48h,

and at 1 and 2 weeks in tissue protection, with a significant decrease in apoptosis, a significant increase in neovascularization as well as an increase of the number of proliferative endothelial cells in the lesion core. However, in a rat model of 2h tMCAO others obtained opposite results showing decreased Cav-1 expression at 24, 48 and 72h in the ipsilateral hemisphere[17]. In their study, the decrease in Cav-1 expression was associated with an increase in metalloproteinase activity at 24h after a 15 min tMCAO in Cav-1 KO mice[17]. The discrepancy between our results and Gu and collaborators[17] may be explained by variations in the experimental protocols such as the occlusion time (35min, 1 hour, 3 hours), as well as using two different stroke models in two different species (rat and mouse) as well as the immunoblot analysis of homogenates of the entire ischemic hemisphere versus homogenates of the ischemic core only. In summary, our behavioral outcomes after stroke support the idea that endogenous Cav-1 plays a beneficial role in limiting the extension of the lesion after 35 min tMCAO in mice.

**Benefit from post-stroke neovascularization:**

Studies showed Cav-1 expression in various cell types of the neurovascular unit. In a juvenile rat TBI model, we previously showed an increase in Cav-1 expression in endothelial cells and astrocytes[12]. Observing a decrease in survival of Cav-1 KO animals at 3 to 4 days after TBI and significant signs of recovery in WT animals in the behavioral tests, we explored the localization of Cav-1 protein here at 3 days after tMCAO by immunofluorescence staining in WT animals. Cav-1 was present in CD31 positive endothelial cells. This result is in agreement with previous work, as endothelial cells are one of the cell populations that express the highest level of caveolae and Cav-1 and caveolae are thought to constitute up to 30% of the total endothelial cell surface in capillaries[7]. Interestingly, the ischemic hemisphere appeared to have increased expression of Cav-1 after stroke compared to contralateral hemisphere. This was also seen in previous studies showing increased Cav-1 expression in the ischemic hemisphere after photothrombotic ischemia in mice[27] and tMCAO in rats[19]. But this needed to be confirmed with the more physiological tMCAO model of stroke in mice. Previous studies extensively investigated

the correlation between BBB protection against disruption and Cav-1 expression and thus offering Cav-1 a protective role against BBB breakdown during focal cerebral ischemia[27]. The deficiency of neovascularization in Cav-1 KO mice has already been assessed in a permanent cerebral ischemia model of distal ligation of the MCA[19] and in a hindlimb ischemia model[31]. In the work by Jasmin et al, 2007, PCNA (proliferating cell nuclear antigen)-positive blood vessels were labeled with laminin belonging to the perivascular matrix. Here we present another MCAO model and another marker of cell proliferation, Ki67, to confirm these results. In our tMCAO model, we observed endothelial cell proliferation in the ischemic lesion in both groups of animals (Figure 4a-d) in agreement with previous studies[7]. However, Cav-1 KO mice exhibited significantly less neovascularization with fewer Ki67-positive endothelial cells compared to WT and decreased vessel density. This suggests a lower number of new endothelial cells in the ischemic lesion when Cav-1 is absent. Neovascularization is a dynamic process of endothelial proliferation, migration and differentiation and a well-established event occurring in the ischemic lesion[7]. It is essential for brain recovery as it stimulates blood flow, collateralization and neuroplasticity[31]. The impaired neovascularization might contribute to the increased ischemic injury observed in Cav-1 KO mice. Mechanistically, Cav-1 could act as a "differentiation sensor" to directly modulate regulators of neovascularization, such as vascular endothelial growth factor (VEGF), produced by the astrocytes and eNOS to coordinate proliferation and differentiation of endothelial cells[7].

**Benefit from post-stroke astrogliosis:**

Some studies showed Cav-1 in astrocyte cultures *in vitro*[10, 11] and in an *in vitro* model of ischemia reperfusion (oxygen glucose deprivation/ reoxygenation: OGD-R). To our knowledge, apart from our previous study showing localization of Cav-1 protein in rat astrocytes after juvenile TBI *in vivo*[12] we show here for the first time Cav-1, localization in adult mice astrocytes positive for GS and GFAP after ischemic stroke (Figure 1d-g). However, the emerging view is that astrocytes constitute a heterogeneous population[8] and the role of Cav-1 in astrocytes is unknown in both

normal and pathological brain tissue. Astrogliosis is defined as the response of astrocytes to all forms of brain stress, damage and disease with particular changes in gene expression, cellular structure and functions[8]. Marked diffuse reactive astrogliosis is generally found in areas surrounding severe focal lesions forming a glial scar[33]. This is thought of as part of the first phase after focal injury such as ischemia, comprising cell death and inflammation[34] and may have beneficial effects on brain injury outcome, including neuronal protection, BBB repair and restriction of inflammation[35]. However, the role of Cav-1 in astrocytes has never been considered after ischemia. Notably, we show here morphological differences in reactive astrocytes in the absence of Cav-1. Specifically, the ramification pattern was different between the WT and Cav-1 KO mice with a significant decrease in the total length of segments and the maximum branch length in Cav-1 KO mice. The low level of ramification and process complexity of the Cav-1 KO astrocytes could prevent scar formation. We observed better recovery of WT mice at 3 dpi in behavioral tests while Cav-1 KO animals had sparse reactive astrocytes and absence of a glial scar and reactive morphology in the ischemic peri-lesion. One other study also found less astroglial differentiation in the dentate gyrus of adult Cav-1 KO mice[36] indicating that genetic ablation of Cav-1 may directly inhibit the formation of new reactive astrocytes and be detrimental to the ischemic injury. While traditionally viewed as a barrier to axon regeneration, beneficial functions of the glial scar have recently been identified[37]. An emerging concept is that astrocytic scar could actually aid central nervous system regeneration. In a model of spinal cord injury (SCI), RNA sequencing revealed that astrocytes and non-astrocyte cells in SCI lesions express multiple axon-growth-supporting molecules and by contrast preventing astrocytic scar formation significantly reduced this stimulated axon regrowth[38]. The glial scar has been widely studied in the context of SCI, but it also occurs after traumatic brain injury and ischemic stroke and more work is needed in these models.

Although several studies already investigated Cav-1 signaling pathways of in astrocytes *in vitro*[39-41], the mechanism by which Cav-1 regulates astrogliosis is still unclear. In an *in vitro* model of ischemia – reperfusion (OGD-R), a recent study suggested that basic fibroblast growth factor

(bFGF) might protect astrocytes from injury by up-regulating the Cav-1/VEGF signaling pathway[41]. In addition to the roles of the Cav-1/VEGF signaling pathway in neovascularization and neurogenesis, it may be also involved in astrogliosis, astroglial scar formation and neuroinflammation after cerebral ischemia[41].

<u>Limitations</u>

There are several limitations to the present study. In particular, in-depth mechanistic as to how Cav-1 promotes revascularization and inhibits astrogliosis after stroke remain to be investigated. Also, so far only the full Cav-1 KO mouse model is available but to prove a primary role of Cav-1, deletion of Cav-1 at a delayed time point after infarct resolution using a tamoxifen-inducible conditional deletion of Cav-1 would be very interesting. Likewise, manipulation by specific knock-out or overexpression of Cav-1 in an endothelial-specific manner to rescue revascularization and astrocyte-specific targeting astrogliosis could be interesting approaches.

**Summary**

Altogether, characterization of Cav-1 KO mice brings insight into the role of Caveolin-1 in brain injuries. In this study, we focused on endothelial cells and astrocytes of the neurovascular unit, for a novel perspective on approaches against ischemia injury. We saw better survival after stroke and better recovery of sensorimotor deficits if Cav-1 was present. These results point towards a potential protective role of endogenous Cav-1 in the neurovascular unit in the first days after stroke. Our hypothesis is that via its signaling functions, Cav-1 and caveolae formation could play a role in BBB repair, neovascularization and astrogliosis after ischemic injury. A key protein in 'wound-healing', mimicking caveolin functions could be a novel neuroprotective strategy.

## Acknowledgements

Disclosure of conflicting interest

The authors declare that there is no conflict of interest.


Supplementary material

Supplementary material for this paper is available at:

http://jcbfm.sagepub.com/content/by/supplemental-data.

**References**

1. Mozaffarian D, Benjamin EJ, Go AS, et al. Heart Disease and Stroke Statistics-2016 Update: A Report From the American Heart Association. *Circulation* 2016; 133: e38-360. 2015/12/18. DOI: 10.1161/CIR.0000000000000350.
2. Meadows KL. Experimental models of focal and multifocal cerebral ischemia: a review. *Rev Neurosci* 2018 2018/02/06. DOI: 10.1515/revneuro-2017-0076.
3. Goyal M, Menon BK, van Zwam WH, et al. Endovascular thrombectomy after large-vessel ischaemic stroke: a meta-analysis of individual patient data from five randomised trials. *The Lancet* 2016; 387: 1723-1731. DOI: 10.1016/s0140-6736(16)00163-x.
4. Neuhaus AA, Couch Y, Hadley G, et al. Neuroprotection in stroke: the importance of collaboration and reproducibility. *Brain : a journal of neurology* 2017; 140: 2079-2092. 2017/06/24. DOI: 10.1093/brain/awx126.
5. Zhang JH, Badaut J, Tang J, et al. The vascular neural network--a new paradigm in stroke pathophysiology. *Nat Rev Neurol* 2012; 8: 711-716. 2012/10/17. DOI: 10.1038/nrneurol.2012.210.
6. Persidsky Y, Ramirez SH, Haorah J, et al. Blood-brain barrier: structural components and function under physiologic and pathologic conditions. *Journal of neuroimmune pharmacology : the official journal of the Society on NeuroImmune Pharmacology* 2006; 1: 223-236. 2007/11/28. DOI: 10.1007/s11481-006-9025-3.
7. Xu L, Guo R, Xie Y, et al. Caveolae: molecular insights and therapeutic targets for stroke. *Expert Opin Ther Targets* 2015; 19: 633-650. DOI: 10.1517/14728222.2015.1009446.
8. Sofroniew MV. Astrogliosis. *Cold Spring Harb Perspect Biol* 2014; 7: a020420. 2014/11/09. DOI: 10.1101/cshperspect.a020420.
9. Hnasko RL, M. P. The Biology of Caveolae: Lessons from Caveolin Knockout Mice and Implications for Human Disease. *Mol Interv* 2003; 3: 20.
10. Ikezu T, Ueda H, Trapp BD, et al. Affinity-purification and characterization of caveolins from the brain: differential expression of caveolin-1, -2, and -3 in brain endothelial and astroglial cell types. *Brain Res* 1998; 804: 177-192. 1998/12/05.
11. Cameron PL, Ruffin JW, Bollag R, et al. Identification of caveolin and caveolin-related proteins in the brain. *The Journal of neuroscience : the official journal of the Society for Neuroscience* 1997; 17: 9520-9535. 1998/01/10.
12. Badaut J, Ajao DO, Sorensen DW, et al. Caveolin expression changes in the neurovascular unit after juvenile traumatic brain injury: signs of blood-brain barrier healing? *Neuroscience* 2015; 285: 215-226. 2014/12/03. DOI: 10.1016/j.neuroscience.2014.10.035.
13. Stern CM and Mermelstein PG. Caveolin regulation of neuronal intracellular signaling. *Cell Mol Life Sci* 2010; 67: 3785-3795. 2010/07/16. DOI: 10.1007/s00018-010-0447-y.
14. Razani BW, S. E.; Lisanti, M. P. Caveolae: From Cell Biology to Animal Physiology. *Pharmacological review* 2002; 54: 37.
15. Okamoto T, Schlegel A, Scherer PE, et al. Caveolins, a family of scaffolding proteins for organizing "preassembled signaling complexes" at the plasma membrane. *The Journal of biological chemistry* 1998; 273: 5419-5422. 1998/04/16.
16. Garcia-Cardena G, Martasek P, Masters BS, et al. Dissecting the interaction between nitric oxide synthase (NOS) and caveolin. Functional significance of the nos caveolin binding domain in vivo. *The Journal of biological chemistry* 1997; 272: 25437-25440. 1997/11/05.
17. Gu Y, Zheng G, Xu M, et al. Caveolin-1 regulates nitric oxide-mediated matrix metalloproteinases activity and blood-brain barrier permeability in focal cerebral ischemia and reperfusion injury. *Journal of neurochemistry* 2012; 120: 147-156. 2011/10/20. DOI: 10.1111/j.1471-4159.2011.07542.x.
18. Gu Y, Dee CM and Shen J. Interaction of free radicals, matrix metalloproteinases and caveolin-1 impacts blood-brain barrier permeability. *Frontiers in bioscience (Scholar edition)* 2011; 3: 1216-1231. 2011/05/31.

19.    Jasmin JF, Malhotra S, Singh Dhallu M, et al. Caveolin-1 deficiency increases cerebral ischemic injury. *Circulation research* 2007; 100: 721-729. 2007/02/13. DOI: 10.1161/01.res.0000260180.42709.29.

20.    Knowland D, Arac A, Sekiguchi KJ, et al. Stepwise recruitment of transcellular and paracellular pathways underlies blood-brain barrier breakdown in stroke. *Neuron* 2014; 82: 603-617. DOI: 10.1016/j.neuron.2014.03.003.

21.    Pawson T and Scott JD. Signaling through scaffold, anchoring, and adaptor proteins. *Science* 1997; 278: 2075-2080. 1998/02/12.

22.    Fluri F, Schuhmann MK and Kleinschnitz C. Animal models of ischemic stroke and their application in clinical research. *Drug Des Devel Ther* 2015; 9: 3445-3454. 2015/07/15. DOI: 10.2147/DDDT.S56071.

23.    Bederson JB, Pitts LH, Tsuji M, et al. Rat middle cerebral artery occlusion: evaluation of the model and development of a neurologic examination. *Stroke* 1986; 17: 472-476.

24.    Hirt L, Badaut J, Thevenet J, et al. D-JNKI1, a cell-penetrating c-Jun-N-terminal kinase inhibitor, protects against cell death in severe cerebral ischemia. *Stroke* 2004; 35: 1738-1743. DOI: 10.1161/01.STR.0000131480.03994.b1.

25.    Balkaya M, Krober JM, Rex A, et al. Assessing post-stroke behavior in mouse models of focal ischemia. *J Cereb Blood Flow Metab* 2013; 33: 330-338. 2012/12/13. DOI: 10.1038/jcbfm.2012.185.

26.    Morrison H, Young K, Qureshi M, et al. Quantitative microglia analyses reveal diverse morphologic responses in the rat cortex after diffuse brain injury. *Scientific reports* 2017; 7: 13211. 2017/10/19. DOI: 10.1038/s41598-017-13581-z.

27.    Choi KH, Kim HS, Park MS, et al. Regulation of Caveolin-1 Expression Determines Early Brain Edema After Experimental Focal Cerebral Ischemia. *Stroke* 2016; 47: 1336-1343. 2016/03/26. DOI: 10.1161/strokeaha.116.013205.

28.    Macrae IM. Preclinical stroke research – advantages and disadvantages of the most common rodent models of focal ischaemia. *British Journal of Pharmacology* 2011; 164. DOI: 10.1111/bph.2011.164.issue-4.

29.    Trushina E, Du Charme J, Parisi J, et al. Neurological abnormalities in caveolin-1 knock out mice. *Behavioural brain research* 2006; 172: 24-32. DOI: 10.1016/j.bbr.2006.04.024.

30.    Gioiosa L, Raggi C, Ricceri L, et al. Altered emotionality, spatial memory and cholinergic function in caveolin-1 knock-out mice. *Behavioural brain research* 2008; 188: 255-262. 2007/12/18. DOI: 10.1016/j.bbr.2007.11.002.

31.    Zhang ZG and Chopp M. Neurorestorative therapies for stroke: underlying mechanisms and translation to the clinic. *The Lancet Neurology* 2009; 8: 491-500. DOI: 10.1016/s1474-4422(09)70061-4.

32.    Sonveaux P, Martinive P, DeWever J, et al. Caveolin-1 expression is critical for vascular endothelial growth factor-induced ischemic hindlimb collateralization and nitric oxide-mediated angiogenesis. *Circulation research* 2004; 95: 154-161. 2004/06/19. DOI: 10.1161/01.RES.0000136344.27825.72.

33.    Sofroniew MV and Vinters HV. Astrocytes: biology and pathology. *Acta Neuropathol* 2010; 119: 7-35. 2009/12/17. DOI: 10.1007/s00401-009-0619-8.

34.    Burda JE and Sofroniew MV. Reactive gliosis and the multicellular response to CNS damage and disease. *Neuron* 2014; 81: 229-248. 2014/01/28. DOI: 10.1016/j.neuron.2013.12.034.

35.    Sofroniew MV. Astrocyte barriers to neurotoxic inflammation. *Nat Rev Neurosci* 2015; 16: 249-263. 2015/04/22. DOI: 10.1038/nrn3898.

36.    Li Y, Lau WM, So KF, et al. Caveolin-1 promote astroglial differentiation of neural stem/progenitor cells through modulating Notch1/NICD and Hes1 expressions. *Biochem Biophys Res Commun* 2011; 407: 517-524. 2011/03/19. DOI: 10.1016/j.bbrc.2011.03.050.

37.    Adams KL and Gallo V. The diversity and disparity of the glial scar. *Nat Neurosci* 2018; 21: 9-15. 2017/12/23. DOI: 10.1038/s41593-017-0033-9.

38.     Anderson MA, Burda JE, Ren Y, et al. Astrocyte scar formation aids central nervous system axon regeneration. *Nature* 2016; 532: 195-200. 2016/03/31. DOI: 10.1038/nature17623.

39.     Jo A, Park H, Lee SH, et al. SHP-2 binds to caveolin-1 and regulates Src activity via competitive inhibition of CSK in response to H2O2 in astrocytes. *PloS one* 2014; 9: e91582. 2014/03/19. DOI: 10.1371/journal.pone.0091582.

40.     Xu L, Wang L, Wen Z, et al. Caveolin-1 is a checkpoint regulator in hypoxia-induced astrocyte apoptosis via Ras/Raf/ERK pathway. *American journal of physiology Cell physiology* 2016; 310: C903-910. 2016/03/25. DOI: 10.1152/ajpcell.00309.2015.

41.     Liu M, Wu Y, Liu Y, et al. Basic Fibroblast Growth Factor Protects Astrocytes Against Ischemia/Reperfusion Injury by Upregulating the Caveolin-1/VEGF Signaling Pathway. *J Mol Neurosci* 2018; 64: 211-223. 2018/01/05. DOI: 10.1007/s12031-017-1023-9.

**Figure legends**

**Figure 1.** (a) Western blot showing the 20 kD band of Cav-1 in WT sham and tMCAO ipsilateral (tMCAO Ipsi) and contralateral (tMCAO Contra) side to the lesion, α-Tubulin band at 50 kD used as control for n=3 animals per condition. Quantification using the mean grey value and normalized against the mean value for Sham. (b) Caveolin-1 expression after tMCAO in relation to the lesion as shown in neuronal MAP-2 staining on a coronal section. (c) Cav-1 (green) co-localizes with CD31-labeled (red) endothelial cells in the striatum ipsilateral (left panel) and contralateral (right panel) to the ischemic lesion at 3 dpi. (d) In the ipsilateral (left panel) and in the contralateral hemisphere (right panel), Cav-1 (green) was also observed (arrowheads) in the GS-positive astrocytes (red). (e) In the peri-lesion region next to the ventricle (left panel) and in the striatum contralateral to the lesion (right panel), Cav-1 (green) was found to co-localize (arrows) in reactive astrocytes stained with GFAP (red). Respective control staining were made using the same markers on Cav-1 KO tissue and are available in supplementary figure 1. Scale bar = 20 μm.

**Figure 2.** Survival and lesion size assessment after 35 min tMCAO in WT and Cav-1 KO mice. Kaplan-Meier survival plot and (b) lesion size at time of sacrifice measured from cresyl violet staining (not shown), box plot show the mean lesion volume ± min/max for WT and Cav-1 KO mice after 35 min tMCAO surgery and the dots individual animals with the time of sacrifice specified on the x-axis. (c) Immunofluorescence staining using MAP-2 (neuronal marker) on coronal slices of WT and Cav-1 KO mice after tMCAO or sham surgery collected respectively 6 hours, 24 hours and 3 days after stroke, lesion delimited by yellow dotted line. Scale bar = 1mm

**Figure 3.** Behavioral assessment (a) Neuroscore assessed on a scale from 0 (no deficit) to 3 (sacrifice) at 1, 4 and 7 dpi. (b) Latency to fall from the Rotarod apparatus expressed as percent of the best baseline performance value (mean ± SD). (c) Time before contact and (d) before removal of the adhesive placed under each paw of the mouse assessed at 2, 4 and 6 dpi and

expressed as the difference between best baseline performance and best test time for each mouse (mean ± SD).

**Figure 4.** Neovascularization in the lesion. (a-d) Immunofluorescence staining with Ki67 (green) and CD31 (red) in WT (a, c) and Cav-1 KO (b, d) mice at 3 days post-MCAO. Scale bar = 1mm. (e) Immunofluorescence staining with Ki-67 (green), CD31 (red) and DAPI counterstaining (blue) in the striatum ipsilateral to the lesion in the WT (left image) and in the Cav-1 KO (right image), scale bar = 20 µm. (f) Quantification of the vessel density showing the ratio of vasculature area to the total image area (individual points, mean and SD) in WT and Cav-1 KO images (g) Quantification (individual points, mean and SD) of the total number of nuclei stained with Ki67 per area (left plot) and the number of nuclei labeled by Ki67 in the vessels per area (right plot) in WT and Cav-1 KOs. n=3 areas per animal with 3 animals per group, 20x sections.

**Figure 5.** (a) Astrocyte reactivity time-course on coronal brain sections from WT and Cav-1 KO mice stained with GFAP and MAP-2. Sections were collected for sham animals and 6 hours, 1 and 3 days after tMCAO. Scale bar = 1mm (b) Immunofluorescence staining with proliferating cells marker Ki67 (green), reactive astrocytes marker GFAP (red) and DAPI nuclei counterstaining (blue) in the striatum ipsilateral to the lesion in the WT (top image) and in the Cav-1 KO (bottom image), scale bar = 20 µm (c) High magnification (40x) panels on sections obtained at 3 dpi illustrating GFAP positive reactive astrocytes (stained in white on black background) in the striatal peri-lesion in WT (top image) and Cav-1 KO )bottom image), scale bar = 20 µm. Inserts with zoom on a single astrocyte from each group. (d) Analysis of astrocytes number and astrocytic morphology by skeletonization: plot of the number of GFAP-positive cells, number of endpoints, total length of the segment and the maximum branch length in WT and Cav-1 KO astrocytes in the peri-lesion. n=4 areas per animal with 3 animals per group.

**Figure 6.** Summary figure of the differences observed between WT and Cav-1 KO mice. Increased lesion size associated with behavior dysfunction such as sensorimotor deficits were observed in parallel to impaired neovascularization in the core of the lesion and impaired astrogliosis more specifically changes in the astrocytes morphology preventing the scar formation in the peri-lesion.

**Supplementary Figure 1. Negative controls for the Caveolin-1 expression after tMCAO showed in Figure 1.** Immunostaining on Cav-1 KO samples showing none or non-specific staining with Cav-1 (green) and no co-localization with CD31-labeled (red) endothelial cells, astrocytes stained with GS in the striatum ipsilateral (left panel) and contralateral (right panel) to the ischemic lesion at 3 dpi and astrocytes stained with GFAP in the perilesion. A negative control is also provided using the secondary antibodies alone for the same conditions. Scale bar = 20 µm.

**Supplementary Figure 2. Caveolin-1 expression after tMCAO in neurons.** Triple immunostaining of Cav-1 (green) and Iba-1 microglial marker (red) and neurons stained with NeuN (grey). Co-localization between Cav-1 can be observed with neurons in the peri-lesion (right panel) showed with yellow arrows but not in microglia. Scale bar = 20 µm.

**Supplementary Figure 3.** Comparison of the behavioral tests performed in WT and Cav-1 KO mice after sham injury. (a) Latency to fall from the Rotarod apparatus expressed as percent of the best baseline value before sham surgery. (b) Time before contact and (c) before removal of the adhesive placed under each paw of the mouse assessed on days 2, 4 and 6 after sham surgery and expressed as the difference between best baseline and best test time for each mouse. No significant difference was found in the two-way ANOVA with repeated measures. (mean ± SD)

**Supplementary Figure 4.** Neuroscore assessed on a scale from 0 (no deficit) to 3 (sacrifice) on each day following stroke until planned sacrifice at day 7 post-tMCAO. No significant difference was highlighted by the 2-way ANOVA with repeated measures.

**Supplementary Figure 5.** Identification of the other cell types stained for Ki67. Triple immunostaining with Ki67 (green), Iba1 (red), GFAP (grey) and nuclear counter-staining with DAPI (blue) in the periphery of the lesion showing new proliferating microglial cells stained with Iba1 in the lesion and Ki67 (white arrows) as well as new proliferating reactive astrocytes GFAP and Ki67 positive (yellow arrowheads) in the peri-lesion for the WT (left panel) and the Cav-1 KO (right panel).
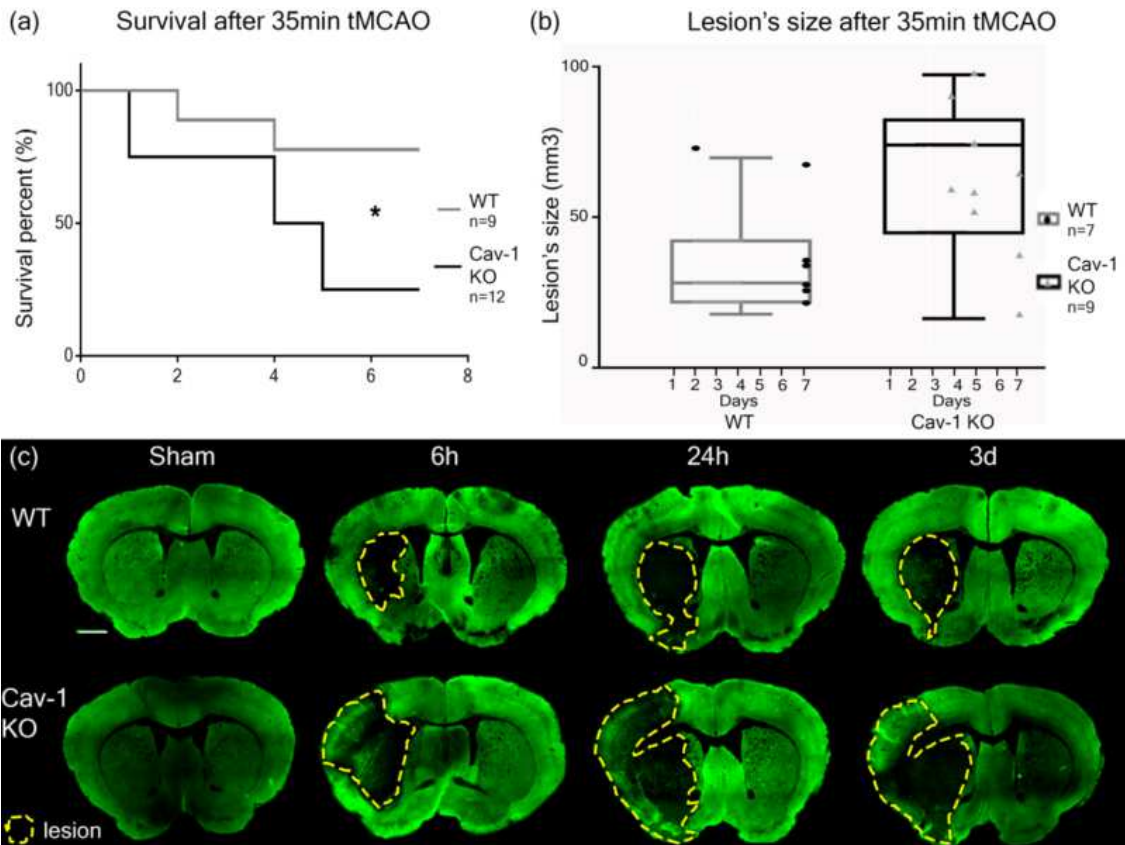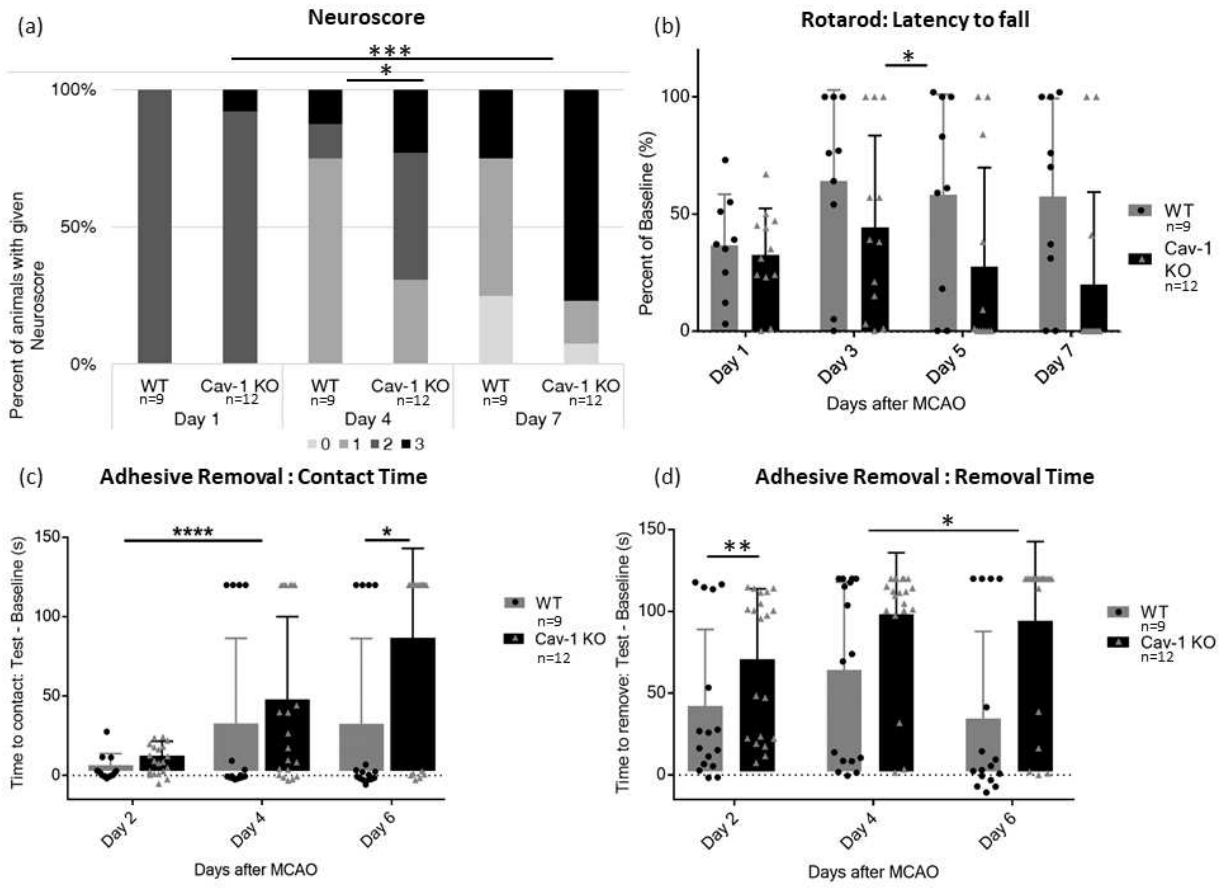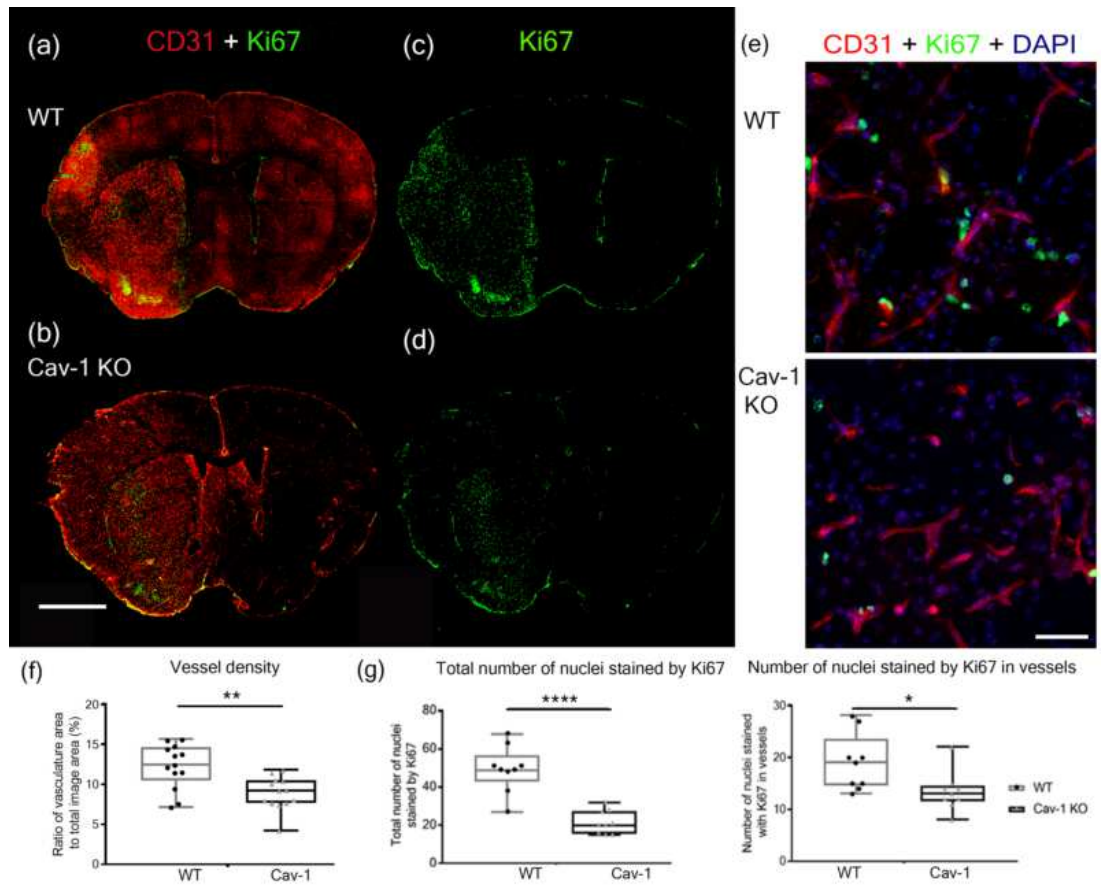
Fig. 1



Fig. 2

Fig. 3



Fig. 4

Fig. 5

tMCAO 3d

WT　　　　　　　　Cav-1 KO



lesion
vessels
astrocytes

Impaired neovascularization

Impaired astrogliosis

Lesion size & behavior dysfunction & mortality

Fig. 6